Journal of Alloys and Compounds 504 (2010) 330–340

Contents lists available at ScienceDirect

Journal of Alloys and Compounds

journal homepage: www.elsevier.com/locate/jallcom

Effect of the addition of Ta on microstructure and properties of Ti–Nb alloys

S.A. Souza[a,*], R.B. Manicardi[a], P.L. Ferrandini[b], C.R.M. Afonso[c], A.J. Ramirez[c], R. Caram[a]

[a] Department of Materials Engineering, Faculty of Mechanical Engineering, State University of Campinas, 13083-970 Campinas, SP, Brazil
[b] Metalpart Ltda, 09991-110 Diadema, SP, Brazil
[c] Electron Microscopy Laboratory, Brazilian Synchrotron Light Laboratory, 13083-970 Campinas, SP, Brazil

ARTICLE INFO

Article history:
Received 15 February 2010
Received in revised form 20 May 2010
Accepted 28 May 2010
Available online 8 June 2010

Keywords:
Metals and alloys
Microstructure
X-ray diffraction

ABSTRACT

This work is a study of the microstructures and properties of a series of Ti–*x*Nb–*y*Ta alloys (*x* = 25, 30, 35; *y* = 0, 2.5, 5, 7.5) (wt. %), solution treated and cooled under the following conditions: furnace cooling (FC), air cooling (AC), oil quenching (OQ) and water quenching (WQ). The results showed the existence of a high density of ω precipitates in FC and AC samples. The microstructures of OQ and WQ alloys containing 25 and 30 wt.% Nb were basically formed by α″ martensite and Ti–35Nb–7.5Ta was the only composition where the β phase was entirely retained. In FC and AC samples, ω phase was most responsible for the high values of elastic modulus and hardness, whereas the OQ and WQ samples showed a continuous decrease in elastic modulus due to the high β retention as the content of alloying elements increased; the WQ sample of composition Ti–35Nb–7.5Ta presented the lowest value of elastic modulus (64 GPa). Hardness tends to decrease with Ta additions. Reduction in area seemed to be independent on Nb and Ta contents but mechanical strength decreased as Nb and Ta percentages increased. Some alloys showed low reduction in area as a consequence of a combination of irregular ω phase distribution and oxygen contamination; these alloys presented the β phase preferably retained at the periphery of specimens, which is attributed to the fall of M_s due to the influence of the cooling rate in Ti-alloys containing Nb and Ta elements, since the higher cooling rate are obtained superficially, and the effect of the oxygen contamination.

1. Introduction

Titanium alloys have been extensively used for decades in aerospace and chemistry industries due to their high specific strength and excellent corrosion resistance [1,2]. Special attention has been directed to orthopedic implants where β-type alloys stand out because of higher biocompatibility [3,4]. In this context, additions of Nb and Ta to Ti are usual based on their biological passivity and capacity of reducing the elastic modulus [5–9]. These elements are widely utilized in combination with Zr, Sn and Mo [10–12].

At room temperature, stable phases in Ti–Nb and Ti–Ta alloys are α (hcp) and β (bcc). During the decomposition of the β phase, in processes that occur out of equilibrium, metastable phases can be formed such as α′ (hexagonal), α″ (orthorhombic) and ω (hexagonal); α′ and α″ are martensitic phases and ω can be formed either by nucleation and growth during aging or plane collapse of the bcc structure along the [1 1 1] direction upon quenching [13–15]. ω phase precipitation has not been observed in Ti–Ta quenched alloys despite attempts to identify it [16,17]. The presence of these metastable phases depends on the composition and specific conditions of heat treatments and/or cooling rates. In the Ti–Nb system, the α′/α″ transition occurs at 10.5 wt.% Nb [18], and at 36.7 wt.% Nb, the martensitic transformation is completely suppressed [19]. Regarding the Ti–Ta system, the contents are 40 and 67 wt.% Ta, respectively [20,19], but a slight discrepancy is found in the literature [21–23].

A few works are found in the literature on the Ti–Nb–Ta alloys [1,15,24], especially dealing with low tantalum concentrations. Therefore, based on the necessity of understanding the wide range of microstructures that form in titanium alloys and their influence on properties, the purpose of this paper is to examine the microstructures and properties of a series of Ti–*x*Nb–*y*Ta alloys (*x* = 25, 30, 35; *y* = 0, 2.5, 5, 7.5) (wt.%), which were heat treated and cooled under different cooling rates.

2. Experimental procedure

All compositions in this text are given in weight percentage. High purity elements, CP Ti (99.84%), Nb (99.99%) and Ta (99.90%), were arc melted in an argon atmosphere using a water-cooled copper hearth; the ingots obtained were melted at least six times, being flipped between each melt. Then they were encapsulated in quartz tubes under a partial argon atmosphere, homogenized at 1000 °C for 24 h, and furnace cooled. The homogenized ingots were hot-rolled at 900 °C in order to obtain 5 mm thick plates; several rolling operations were necessary and the ingots were reheated before each one. Afterwards, they were mechanically and

* Corresponding author. Tel.: +55 19 3521 3310; fax: +55 19 3521 3314.
E-mail address: sasouza.sandra@gmail.com (S.A. Souza).

0925-8388/$ – see front matter © 2010 Elsevier B.V. All rights reserved.
doi:10.1016/j.jallcom.2010.05.134

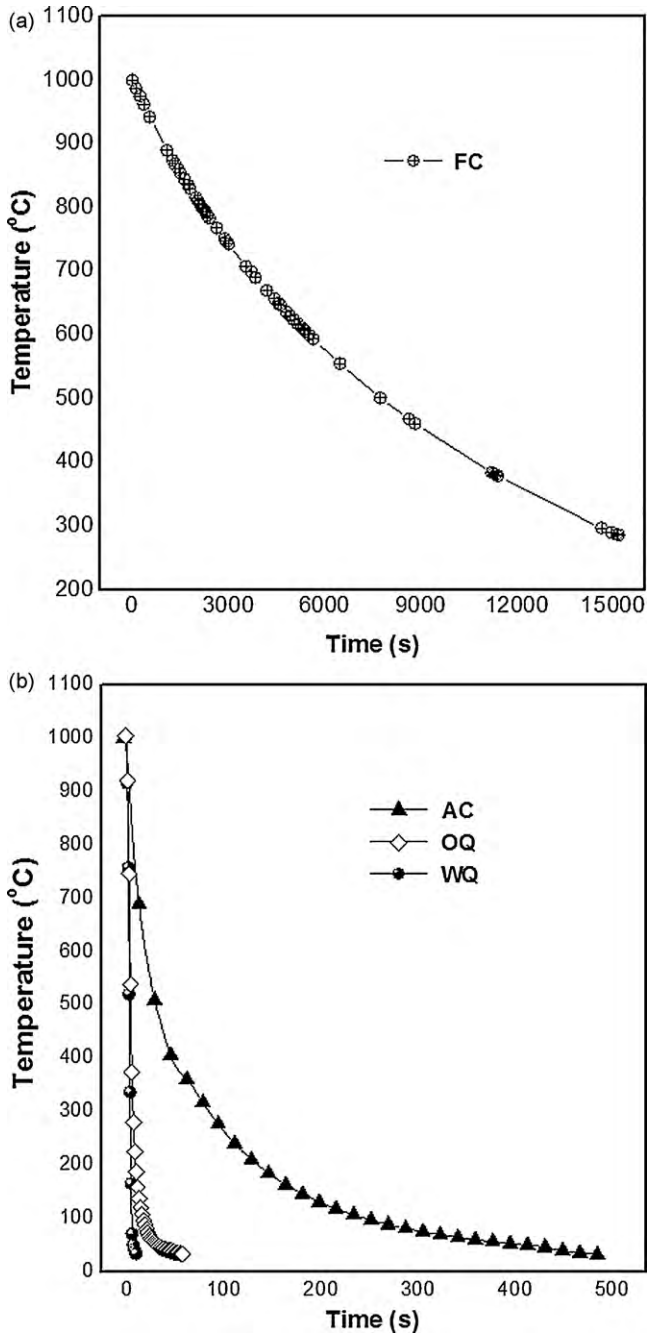

Fig. 1. (a) Curve resulting from furnace cooling (FC) and (b) curves resulting from air cooling (AC), oil quenching (OQ) and water quenching (WQ).

chemically cleaned to remove the layers of oxide, and cut in order to obtain four samples for each composition. The dimensions of each sample were (25 × 20 × 4) mm. Finally, the samples were encapsulated in quartz tubes and heated at 1000 °C/1 h (solution treated) and then cooled under the following conditions: furnace cooling (FC), air cooling (AC), oil quenching (OQ) and water quenching (WQ). Except for the FC samples, all the tubes were broken before cooling. The cooling curves for each condition were obtained through preliminary experiments (Fig. 1) using samples with the same thickness (4 mm). The cooling rates (Table 1) were estimated by linearly fitting the cooling curves in the temperature range from 800 °C to 500 °C.

Table 1
Cooling rates estimated by linearly fitting the cooling curves in the temperature range of 700–500 °C. FC: furnace cooled; AC: air cooled; OQ: oil quenched; WQ: water quenched.

Cooling condition	FC	AC	OQ	WQ
Cooling rate (°C/s)	0.05	11	130	200

Table 2
Phases identified by X-ray diffraction analysis in solution treated alloys. FC: furnace cooled; AC: air cooled; OQ: oil quenched; WQ: water quenched.

Nominal content (wt.%)	Phases present (XRP)			
	FC	AC	OQ	\VQ
Ti–25Nb	α,β	α″,α	α″	α″
Ti–25Nb–2.5Ta	α,β	α″,α	α″	α″
Ti–25Nb–5Ta	α,β	α″,α,β,ω	α″,β	α″
Ti–25Nb–7.5Ta	α,β	β,α″,α,ω	α″,β	α″
Ti–30Nb	α,β,ω	β,α,ω	α″,β	α″
Ti–30Nb–2.5Ta	α,β,ω	β,α,ω	α″,β	α″
Ti–30Nb–5Ta	α,β,ω	β,α	α″,β	α″
Ti–30Nb–7.5Ta	β,α,ω	β,α	α″,β	α″
Ti–35Nb	β,α,ω	β,α	α″,β	α″
Ti–35Nb–2.5Ta	β,α,ω	β,α	α″,β	α″
Ti–35Nb–5Ta	β,α	β,α	β,α″	β,α″
Ti–35Nb–7.5Ta	β	β	β	β

Other ingots were obtained for tension testing following the procedures of homogenization described above. The ingots were hot-swaged at 900 °C and reheated before each swaging operation. The 4 mm diameter tensile specimens were machined from the swaged ingots. They were encapsulated in quartz tubes, solution treated at 1000 °C/1 h and then some were oil quenched and some water quenched. The quartz tubes were broken before quench. Three tensile tests were performed for each condition.

Optical metallography was carried out on samples, which were mounted and ground using a series of SiC sandpapers from 400 to 1200; they were then polished with diamond suspension from 6 to 0.25 μm using ethyl alcohol as a lubricant, and etched with Kroll's solution, consisting of 5 vol.% HF acid, 30 vol.% HNO_3 acid and 65 vol.% H_2O. Scanning Electron Microscopy (SEM) utilized a JEOL JXA 840A microscope. Samples for Transmission Electron Microscopy (TEM) were ground down to ~80 μm, dimpled down to ~7 μm and ion milled. A JEOL JEM 3010 URP microscope was utilized for TEM analysis. The characterization of samples by X-ray diffraction was performed using a Rigaku DMAX 2200 equipment (40 kV, 30 mA), in Bragg–Brentano reflection geometry with Cu Kα radiation (λ = 1.5418 Å); the data were obtained between 30° and 90° 2θ in steps of 0.02° with counting time of 2 s. Vickers microhardness and hardness were obtained using loads of 200 gf and 10 kgf, respectively; the values reported are the average of five measurements. Elastic moduli were determined using standard through-transmission techniques with wet coupled 6.35 mm longitudinal and shear transducers.

3. Results and discussion

3.1. Furnace cooled samples

The micrographs of the FC samples containing 25% Nb are shown in Fig. 2a and b. The corresponding X-ray diffraction results are shown in Table 2, which presented α and β phases; β was identified by optical microscopy only in the samples containing 5 and 7.5% Ta, as can be seen in the detail in Fig. 2b. This detail presents a grain boundary region under higher magnification revealing the β phase surrounded by α-needles. The volume fraction of the β phase increased slightly for increasing tantalum contents and thus the microstructure of the Ti–25Nb–7.5Ta alloy is highly similar to that of the Ti–25Nb–5Ta alloy. It was observed that the increase in the volume fraction of β obtained with a further addition of 5% Nb to the Ti–25Nb alloy (Fig. 2a and c) was higher than that obtained with the identical increase in the Ta content (Fig. 2a and b). There are similarities between these observations and those described by Dobromyslov and Elkin [19], who showed that the β-stabilizing effect of Nb is stronger than that of Ta when considering binary titanium alloys. Such as occurs with Zr, the effect of Ta could be different in ternary titanium alloys. Zr is known by its neutral behavior [25,26], but its β-stabilizing effect has been underscored [15,24,27] since it becomes stronger when added in conjunction with other β-stabilizing elements such as Nb [27].

The samples containing 30% Nb presented an irregular distribution of α precipitates, as can be seen in Fig. 2d, where α appears preferentially at large grains, probably resulting from migration of

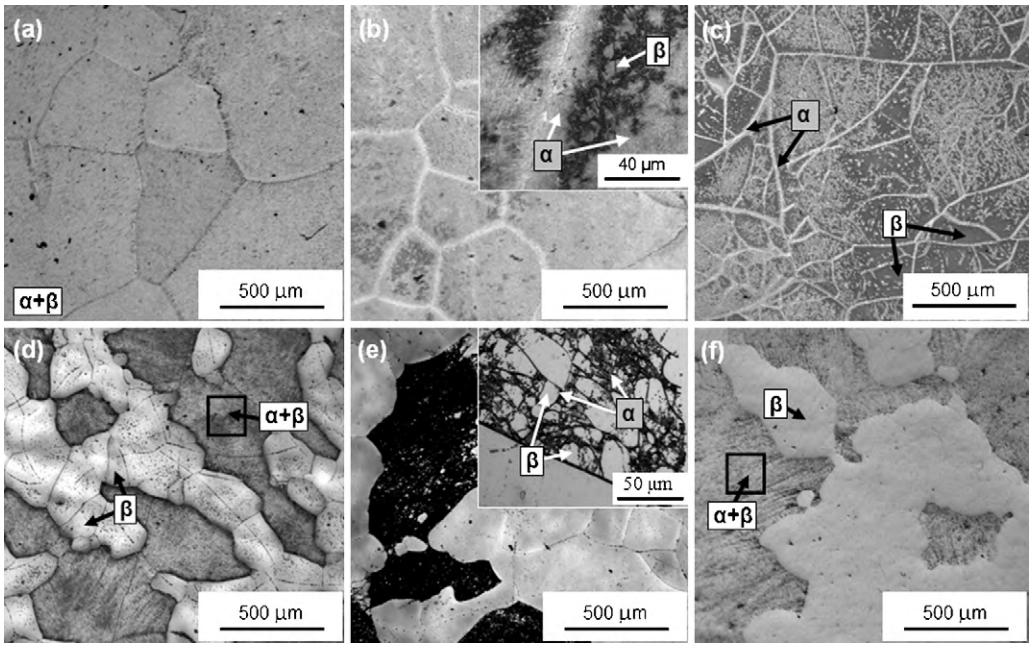

Fig. 2. Optical microscopy of furnace cooled samples. (a) Ti–25Nb, (b) Ti–25Nb–5Ta, (c) Ti–30Nb, (d) Ti–30Nb–7.5Ta, (e) Ti–35Nb, (f) Ti–35Nb–7.5Ta.

low angle boundaries during hot deformation [28]. At large grains, the precipitation occurs simultaneously within the grains and at the grain boundaries [29]. The samples containing 35% Nb are mainly composed by β phase (Fig. 2e and f), but the dark heavily etched areas show that dense precipitation of fine α-particles has occurred in some grains.

The presence of the ω phase was detected by X-ray diffraction in all the samples containing 30% Nb and also in the compositions Ti–35Nb and Ti–35Nb–2.5Ta (Table 2 and Fig. 3a and b). However, the TEM analysis showed that ω phase was also formed in the two FC samples with the highest contents of alloying elements, Ti–35Nb–5Ta and Ti–35Nb–7.5Ta (Fig. 4). A dark field image of the Ti–35Nb–5Ta sample shows ω precipitates finely dispersed within the β matrix (Fig. 4a). Fig. 4b shows the corresponding selected-area diffraction pattern (SADP) and the orientation relationship between β and ω is $[1\bar{1}0]_\beta//[11\bar{2}0]_\omega$. Fig. 4c and d presents the results of the TEM analysis of the Ti–35Nb–7.5Ta sample. The SADP shows the $[315]_\beta$ zone axis, where the reflections of two variants of ω are found: $[1\bar{2}13]$ (ω_1) and $[\bar{1}2\bar{1}3]$ (ω_2).

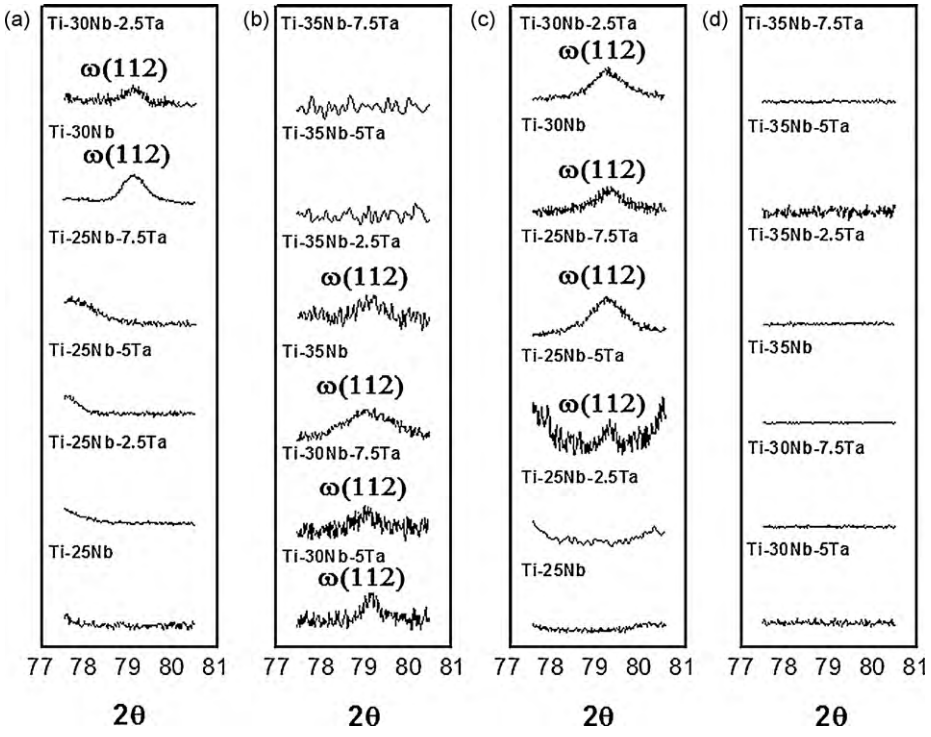

Fig. 3. X-ray diffraction patterns showing the peaks of the ω phase identified in furnace cooled samples (a and b) and air cooled samples (c and d). Lattice parameters of the ω phase: $a = 0.4646$ nm and $c = 0.2820$ nm.

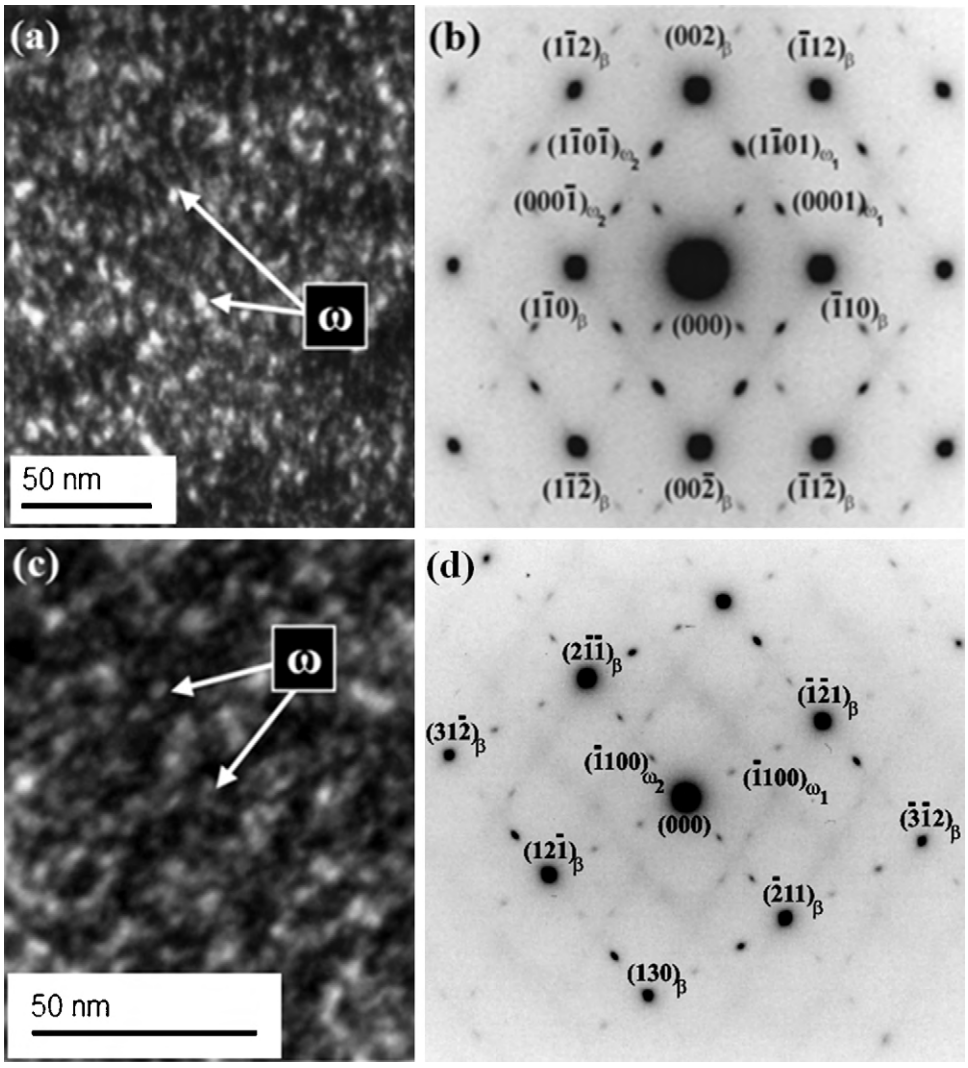

Fig. 4. TEM observations of furnace cooled samples. (a) Dark field image showing ω precipitates in the Ti–35Nb–5Ta alloy and (b) corresponding SADP with $[1\ \bar{1}\ 0]_\beta$ and $[1\ 1\ \bar{2}\ 0]_\omega$ zone axes; (c) Dark field image showing ω precipitates in the Ti–35Nb–7.5Ta alloy and (d) corresponding SADP with $[3\ 1\ 5]_\beta$ zone axis. In this SADP, two crystallographic variants of ω are found: $[1\ \bar{2}\ 1\ 3]_{\omega 1}$ and $[\bar{1}\ 2\ \bar{1}\ 3]_{\omega 2}$ reflections.

Hon et al. [30], who worked with Ti–Nb alloys, reported that ω is found in FC samples of compositions ranging from 26 to 34% Nb. The samples of compositions Ti–25Nb–5Ta and Ti–25Nb–7.5Ta presented relatively high hardness values (∼330 HV) at the regions where intense β-retention was observed, whereas in the regions that presented high density of α precipitates the average value was 270 HV. Although ω phase was not identified, the hardness values found at the regions of intense β-retention were attributed to it, which is consistent with other reported results [31–33].

3.2. Air cooled samples

Fig. 5 shows the microstructures of the samples heated to 1000 °C and air cooled (AC); the cooling rate was estimated to be 11 °C/s (Table 1). X-ray diffraction analysis (Table 2) showed the presence of the α, β, α″ and ω phases in the alloys containing 25% Nb, which also presented more intense morphological variation than other compositions. It is well known that the β → α transformation involves elemental partitioning and makes β phase richer in β-stabilizing elements [15]; however, when the enrichment is insufficient, the martensite may form due to being more stable than β [34]. Thus, the β phase of the samples containing 25% Nb completely transformed to α″ for Ta contents of 0 and 2.5% and partially transformed for Ta contents of 5 and 7.5% (Table 2 and Fig. 5a, b and c). The sample of composition Ti–25Nb–7.5Ta presented a strong reduction in the volume fraction of α″ and its microstructure was almost entirely formed by β phase (Fig. 5c). No α″ martensite was seen in the microstructure of the samples containing higher percentages of alloying elements (Table 2).

In the retained β matrix, ω precipitation was identified through X-ray diffraction in four compositions: Ti–25Nb–5Ta, Ti–25Nb–7.5Ta, Ti–30Nb and Ti–30Nb–2.5Ta (Fig. 3c and d). It could be detected in samples of other compositions, but the continuous increase of the content of alloying elements reduces the ω-precipitate density and therefore diminishes the potential for its detection by XRD. Although ω precipitation is favored under slow cooling rates [35], the rejection from ω phase of alloying elements causes enrichment of β matrix and β becomes more stable as the addition of elements is higher [36]. The formation of ω by solute diffusion also occurs in aging heat treatments, when it is usually named as isothermal ω [37]. According to Tang et al. [15], there is some contribution of a displacive mechanism, which characterizes the formation of athermal ω, during continuous cooling.

In the AC samples (Fig. 5), the morphology of the α precipitates is similar to that observed in the FC sample of composition Ti–35Nb, Fig. 2e. α precipitation decreases gradually as the Nb and

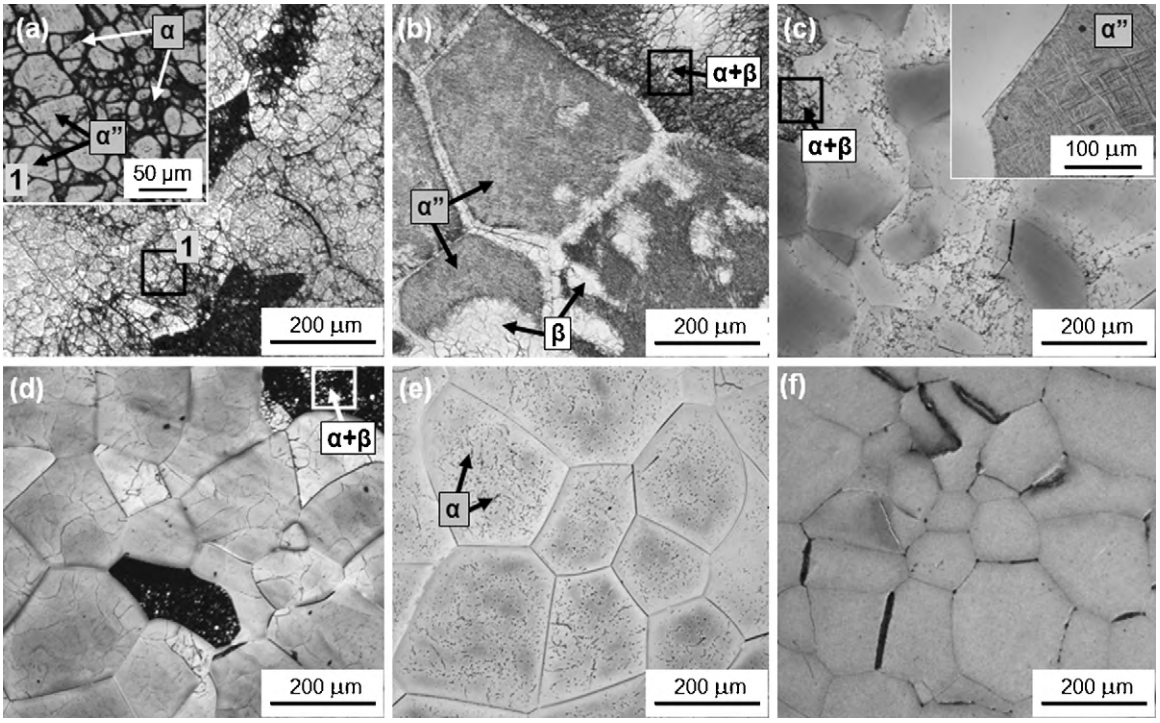

Fig. 5. Optical microscopy of air cooled samples. (a) Ti–25Nb, (b) Ti–25Nb–5Ta, (c) Ti–25Nb–7.5Ta, (d) Ti–30Nb, (e) Ti–35Nb–5Ta, (f) Ti–35Nb–7.5Ta.

Ta contents increase; in the sample of composition Ti–35Nb–7.5Ta (Fig. 5f), it completely disappears and only β phase remains.

3.3. Oil- and water-quenched samples

The microstructures of oil quenched (OQ) samples are shown in Fig. 6. Many features observed are similar to those presented by the water-quenched (WQ) samples. In both conditions, the X-ray diffraction analysis indicated the presence of α″ and β phases, Table 2. Only a slight reduction in the volume fraction of the α″ phase was observed due to the increase in the quenching rate from 130 to 200 °C/s (Table 1). The oil- and water-quenched microstructures of the samples of compositions Ti–25Nb and Ti–25Nb–2.5Ta presented only α″ martensite (see Fig. 6a and b for OQ samples). The observation of a microstructure entirely martensitic in the WQ Ti–25Nb sample is consistent with the one observed by Mantani

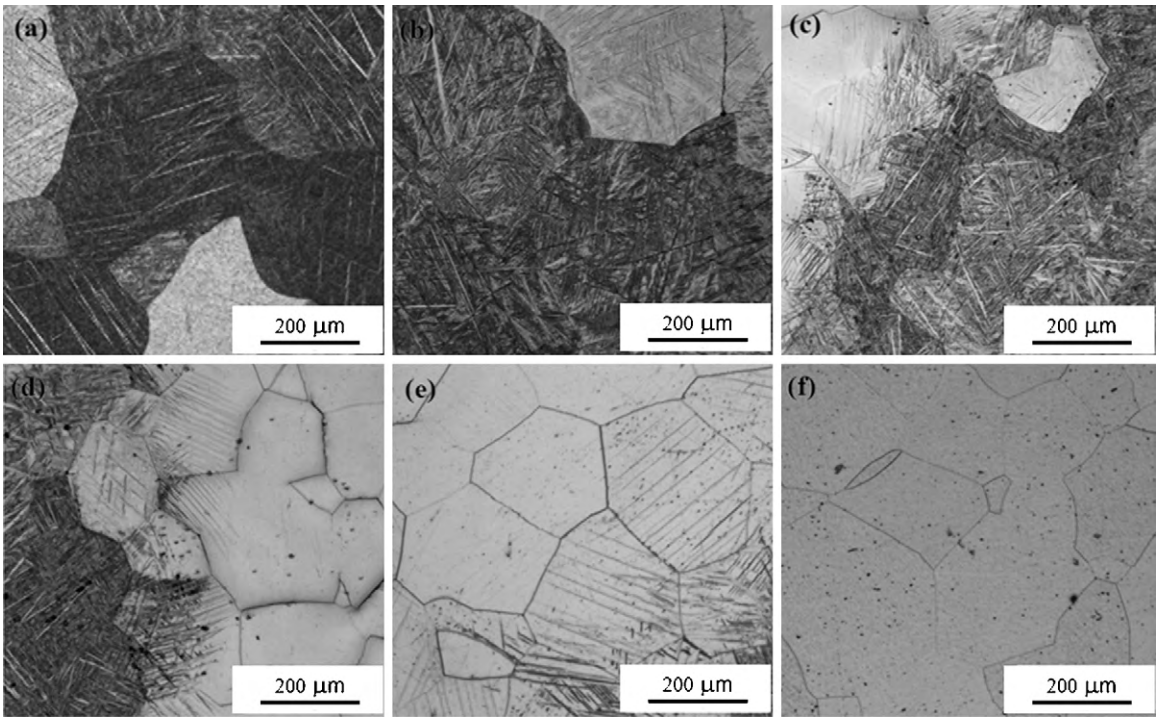

Fig. 6. Optical microscopy of oil quenched samples. (a) Ti–25Nb, (b) Ti–25Nb–2.5Ta, (c) Ti–25Nb–5Ta, (d) Ti–35Nb–2.5Ta, (e) Ti–35Nb–5Ta, (f) Ti–35Nb–7.5Ta.

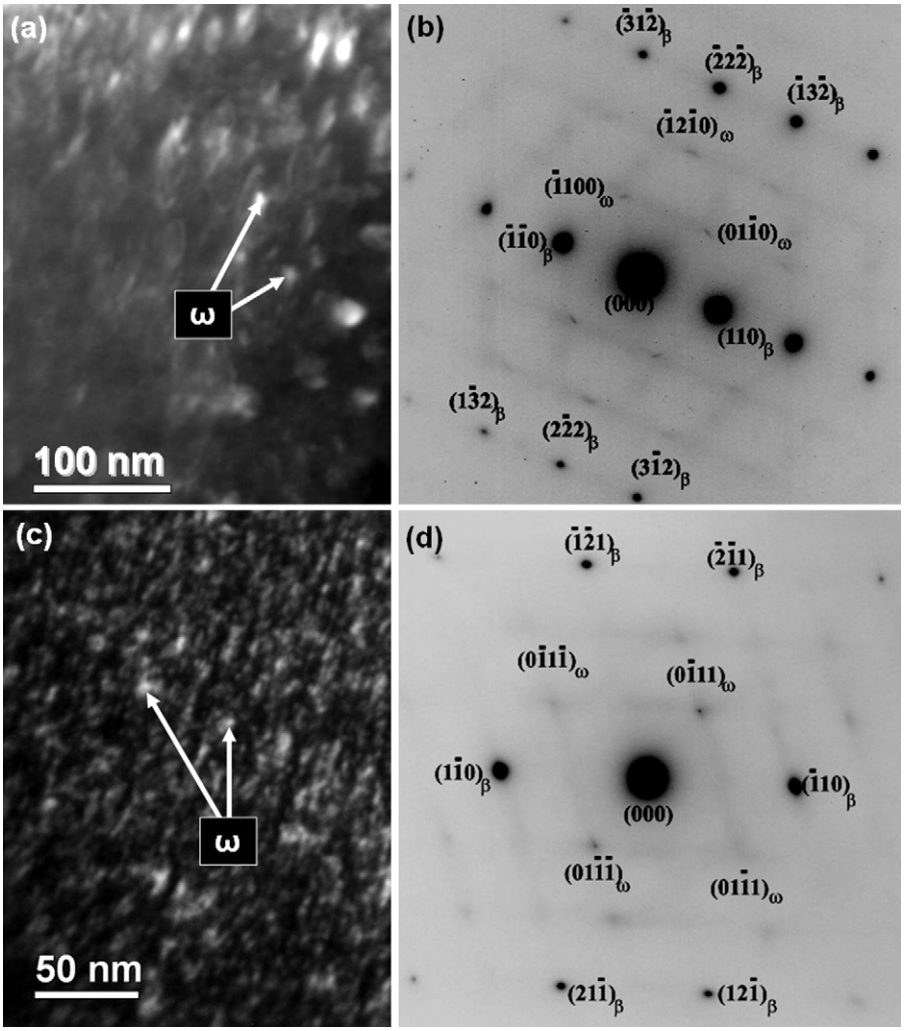

Fig. 7. TEM observations of water-quenched samples. (a) Dark field image showing ω precipitates in the Ti–35Nb–5Ta alloy and (b) corresponding SADP with $[1\ 1\ \bar{2}]_\beta$ zone axis; (c) dark field image showing ω precipitates in the Ti–35Nb–7.5Ta alloy and (d) corresponding SADP with $[1\ 1\ 3]_\beta$ and $[2\ \bar{1}\ \bar{1}\ 0]_\omega$ zone axes.

and Tajima [38]. However, a small β-retention was observed in the WQ specimen with the same composition, Fig. 10a. A possible explanation for this is dealt with in Section 3.5.

The β phase was retained in samples containing 25% Nb when the Ta content was raised to 5%. The aforementioned effect of Ta additions led to gradual β retention, and the samples containing 30% Nb presented a considerably high volume fraction of α″ in both conditions. More significant alterations in the volume fractions of the phases were observed in samples containing 35% Nb (see Fig. 6d, e and f for OQ samples). The microstructure of the sample containing 5% Ta was almost entirely formed by β phase (Fig. 6e). In the alloy of composition Ti–35Nb–7.5Ta, β phase was completely retained, since the martensite start temperature, M_s, is below room temperature.

No evidence of the occurrence of ω phase was detected by X-ray diffraction (Table 2), but the bright-field TEM image of the WQ sample of composition Ti–35Nb–5Ta (Fig. 7a) shows ω precipitates in the β matrix along $[\bar{1}\ 1\ 2]_\beta$ zone axis, Fig. 7b. ω phase was also observed in the sample of composition Ti–35Nb–7.5Ta (Fig. 7c and d). The corresponding SADP gives the β and ω refletions from $[1\ 1\ 3]_\beta$ and $[2\ \bar{1}\ \bar{1}\ 0]_\omega$ zone axes.

3.4. Modulus and hardness

Fig. 8a shows the hardness and elastic modulus values of FC samples as a function of Nb and Ta contents. One observes an initial rise and subsequent fall of the values as the content of alloying elements increase. Among all FC samples, that of composition Ti–30Nb–5Ta presented the highest values of elastic modulus (108 GPa) and hardness (334 HV), Fig. 8a. Its microstructure is comprised of α, β and ω phases (Table 2). The elastic constants of the β-Ti-alloys present a minimum around the M_s. As mentioned in the Section 3.2, the formation of ω leads to an enrichment of the alloying elements in the β matrix. In general, when the M_s of the β matrix is lowered by the enrichment, the elastic modulus increases. However, the enrichment of Nb and Ta causes an increase in lattice parameter of the β phase [19]; the modulus is not only related to the crystal structure, but also to the interatomic distances in the crystal lattice. Therefore, raising Nb and Ta contents of the β phase reduces its elastic modulus. Regarding the ω phase, it has been reported that it has the highest elastic modulus among all the phases in Ti-alloys [32,39–42]. In addition, the ω phase plays a significant role in increasing the hardness [31–33]. Therefore, the ω presence determines the hardness and modulus profiles in Fig. 8a. At first, the high density of its precipitates determines the high values, which continuously decrease; as the content of β-stabilizing elements increases, β becomes more stable and the volume fraction of ω decreases.

The influence of Nb and Ta contents on the hardness of the AC samples showed a trend similar to that presented by the FC samples (Fig. 8a and b). The main difference is that the highest hardness value (349 HV) was found for a lower concentration of alloying ele-

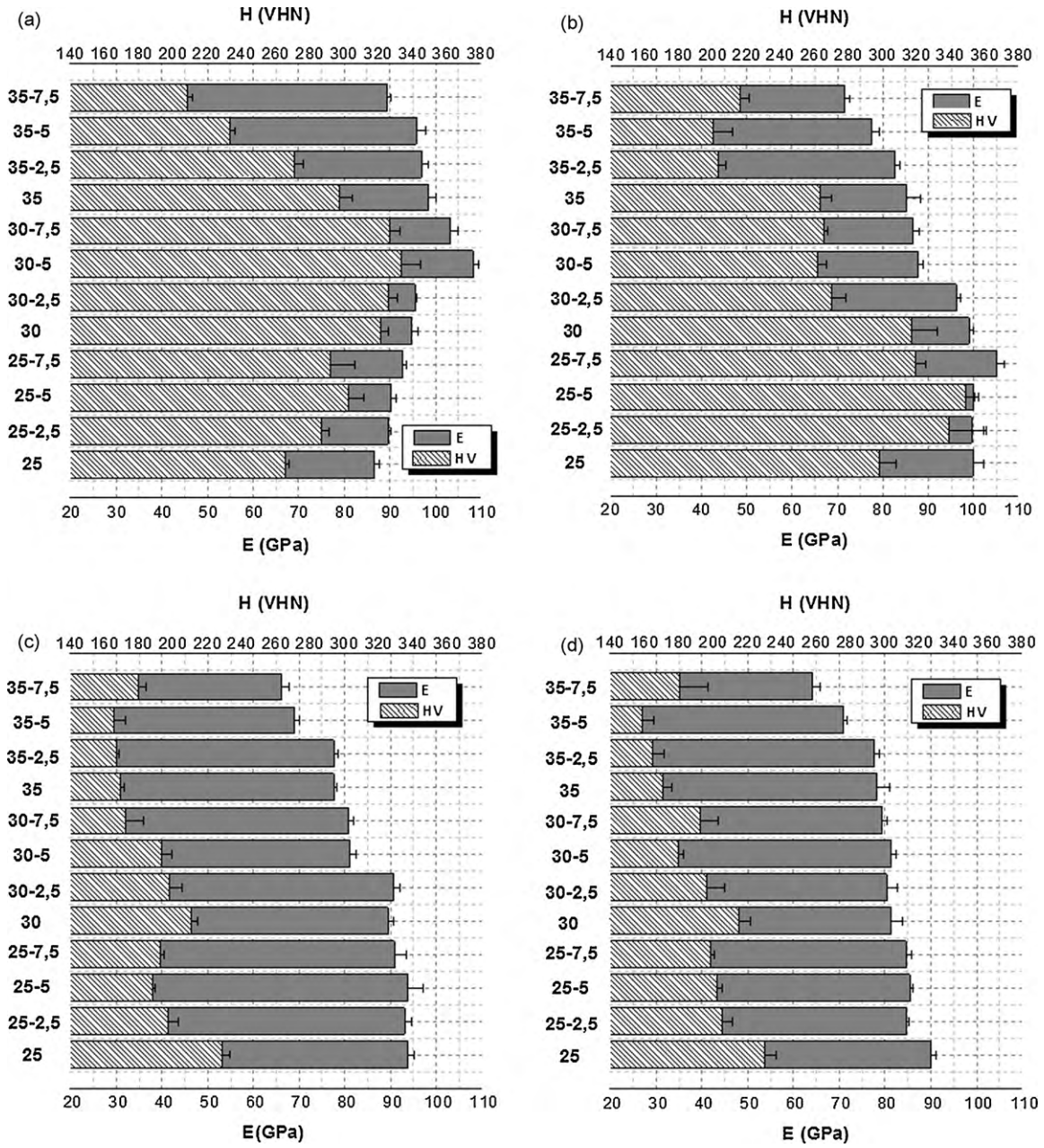

Fig. 8. Elastic modulus and hardness of solution treated alloys. (a) Furnace cooled, (b) air cooled, (c) oil quenched, (d) water quenched. The numbers at the left of each figure correspond to Nb and Ta contents, respectively.

ments, that is, for the sample of composition Ti–25Nb–5Ta, that presented a microstructure composed of α, β, α″ and ω phases (Fig. 8b, Fig. 5b and Table 2). This result is attributed to the increase of the cooling rate from 0.05 to 11 °C/s (Table 1) that hinders nucleation and growth of α phase and favors formation of the harder metastable phases. This finding is supported by the study of Lee et al. [33], who worked with Ti–Nb alloys and said that the hardnesses of the phases are summarized as follows: ω > α″ > β > α. On the elastic modulus, in the AC condition, the sample of composition Ti–25Nb–7.5Ta presented the highest value (105 GPa) and its hardness was also considerably high (319 HV). Again, according to Lee et al. [33], who used three-point bending tests, the moduli of the phases of Ti–Nb alloys can be summarized as follows: ω > α > α″ > β. Hence, one notices that the presence of α influences modulus more than hardness. It is evident that the ω phase has a major role in the elastic modulus and hardness profiles of the FC and AC samples. ω was easily detected in the X-ray diffraction patterns of the samples that presented high values of modulus and hardness, as can be seen in Fig. 3.

The OQ and WQ samples presented relatively low values of elastic modulus (Fig. 8c and d), due to the reduced ω precipitation and α suppression [30,33]. The slightly higher values presented by the OQ samples were attributed to their higher volume fractions of α″ phase. As observed previously, the continuous decrease in elastic modulus observed for increasing Nb and Ta contents is a consequence of higher β retention. A dropping trend in the hardness values is also noticed in Fig. 8c and d when Ta is added to Ti–Nb alloys. However, the alloy of composition Ti–35Nb–7.5Ta in WQ and OQ conditions presented higher hardness values compared with the other alloys containing 35% Nb; solid solution strengthening could be the main reason for this divergence. The WQ sample presented the lowest modulus value (64 GPa), Fig. 8d;

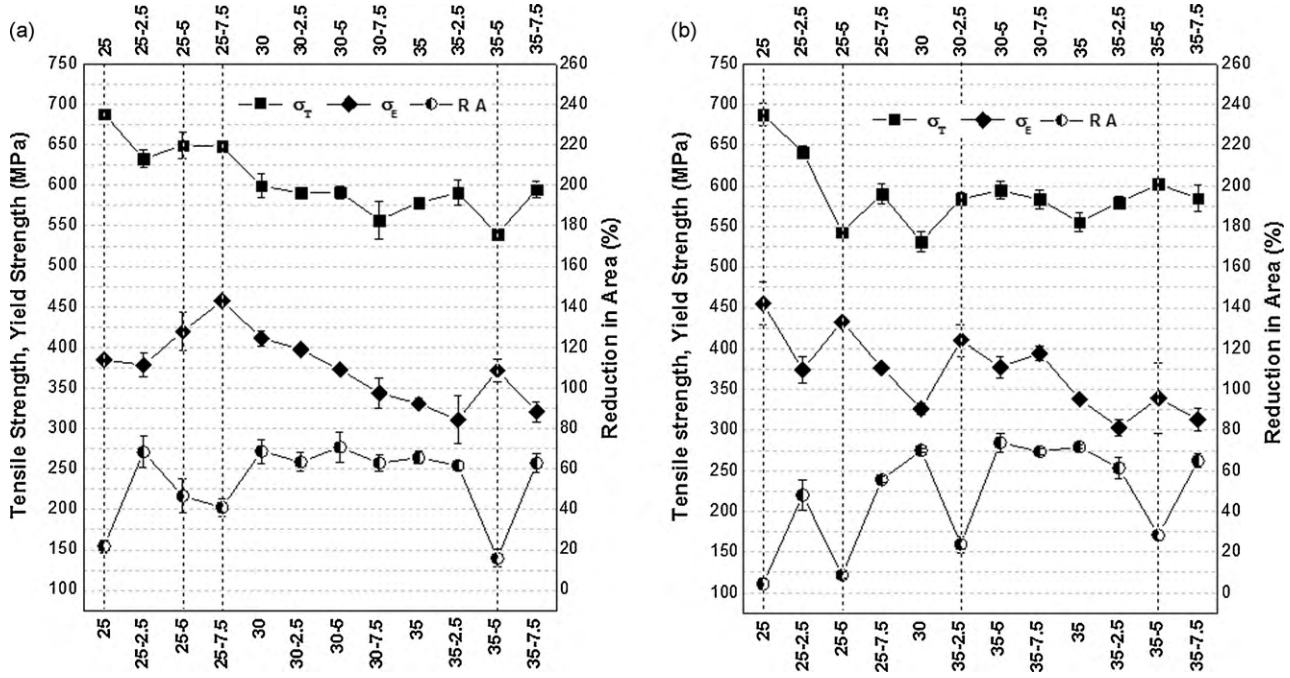

Fig. 9. Tensile properties of solution treated alloys. (a) Oil quenched and (b) water quenched. The dot lines identify the specimens with lower than expected values of reduction in area due to irregular precipitation of the ω phase. The dispersion in the results of the tensile tests is represented by the error bars.

its β-microstructure still contains a small amount of ω precipitates (Fig. 7c and d).

3.5. Tensile properties

Fig. 9 shows tensile properties as a function of Nb and Ta contents in the OQ and WQ conditions, where high ductility and relatively low strength are observed. In this figure, the dispersion in the results of the tensile tests is represented by the error bars. Yield and tensile strength decreased with increasing Nb and Ta contents but the reduction in area seems to be independent of these additions. It can be assumed that the low yield strength is due to the large grain size (ranging from 100 to 400 μm) based on the greater strain hardening of fine grain-sized material compared with a coarse grained polycrystalline aggregate [43]. By way of illustration, Breslauer and Rosen [29] observed that the metastable Ti–15V–3Cr–3Sn–3Al β titanium alloy in non-aged condition presents higher yield strength for small grain-sized specimens (about 35 μm). The alloy of composition Ti–25Nb–7.5Ta in the OQ condition (Fig. 9a) and the alloy of composition Ti–25Nb in the WQ condition (Fig. 9b) presented the highest yield strength (above 450 MPa). For Ti–35Nb–7.5Ta alloy, which presented the lowest elastic modulus value, the yield strength was 313 MPa.

Some specimens, identified with dot lines in Fig. 9, presented considerably low reduction in area; Vickers microhardness measurements were conducted just below the fracture surfaces and the results showed that regions composed of retained β presented the highest values. This fact was observed in other titanium alloys and attributed to the presence of the ω phase [31,33]. ω phase may lead to high strength with reasonable ductility when its volume fraction is controlled. However, uncontrolled ω-phase formation can lead to severe ductility losses [44,45], which is in accordance with the low values of reduction in area seen in Fig. 9.

The WQ specimens containing 25% Nb are particularly useful for analyzing this behavior. They showed the following values of reduction in area: 4% (Ti–25Nb), 48% (Ti–25Nb–2.5Ta), 9% (Ti–25Nb–5Ta) and 56% (Ti–25Nb–7.5Ta). The microstructures below the fracture surfaces of the Ti–25Nb and Ti–25Nb–5Ta specimens are composed by α″ and a small amount of retained β, the latter being observed in the periphery of their cross-sections (Fig. 10a and d). The unexpected β retention in Ti–25Nb specimen as well as the β phase being preferably retained in the periphery is ascribed to the fall of M_s probably due to the higher cooling rate observed superficially. According to Jepson et al. [34], the M_s of the Ti–Nb alloys depends on the cooling rate. Regarding the Ti–Ta alloys, the cooling rate has the same influence on M_s, and therefore, the additions of Ta to Ti–Nb alloys do not cause any alteration on β retention in the periphery of specimens. The cooling rates reported for the OQ and WQ conditions (Table 1) were measured at the centre of the specimens. Therefore, one can state that the peripheral zone of the specimens cooled at a higher cooling rate. Hence, as previously, the higher cooling rate lowers the M_s at the periphery, and higher β retention is observed. Also, oxygen contamination decreases the M_s very effectively and the surface of the specimens can be attacked by oxygen when the quartz tube is broken under water. In Ti–Nb alloys, the addition of O increases phase stability and decreases the elastic modulus, at least of the β phase [46]. Oxygen works in the single β phase alloys, as if it is the β-stabilizing element, although it is still an α-stabilizing element in the aged condition [47]. It is possible, therefore, that the β retention preferably in the periphery is caused by the influence both of the cooling rate and oxygen contamination on the M_s of the Ti-alloys containing Nb and Ta elements.

In general, a regular distribution of β and α″ martensite was observed at the periphery, but some specimens presented a significant and uniform β layer throughout this region, as shown in Fig. 10d. According to Abdel-Hady [47], depending on the composition, the sequence of phase transformation in β-type Ti-alloys is $\alpha'' \rightarrow \alpha'' + \beta + \omega \rightarrow \beta + \omega \rightarrow \beta$. Also, TEM analysis revealed the presence of ω precipitates in the water-quenched specimens of composition Ti–35Nb–5Ta and Ti–35Nb–7.5Ta (Fig. 7). Thus, it is reasonable to say that ω is present in almost all quenched specimens.

Regarding the effect of the oxygen contamination, it is important to highlight that oxygen suppresses the ω phase formation. This is because oxygen operates to pin the linear defects, and hinders the

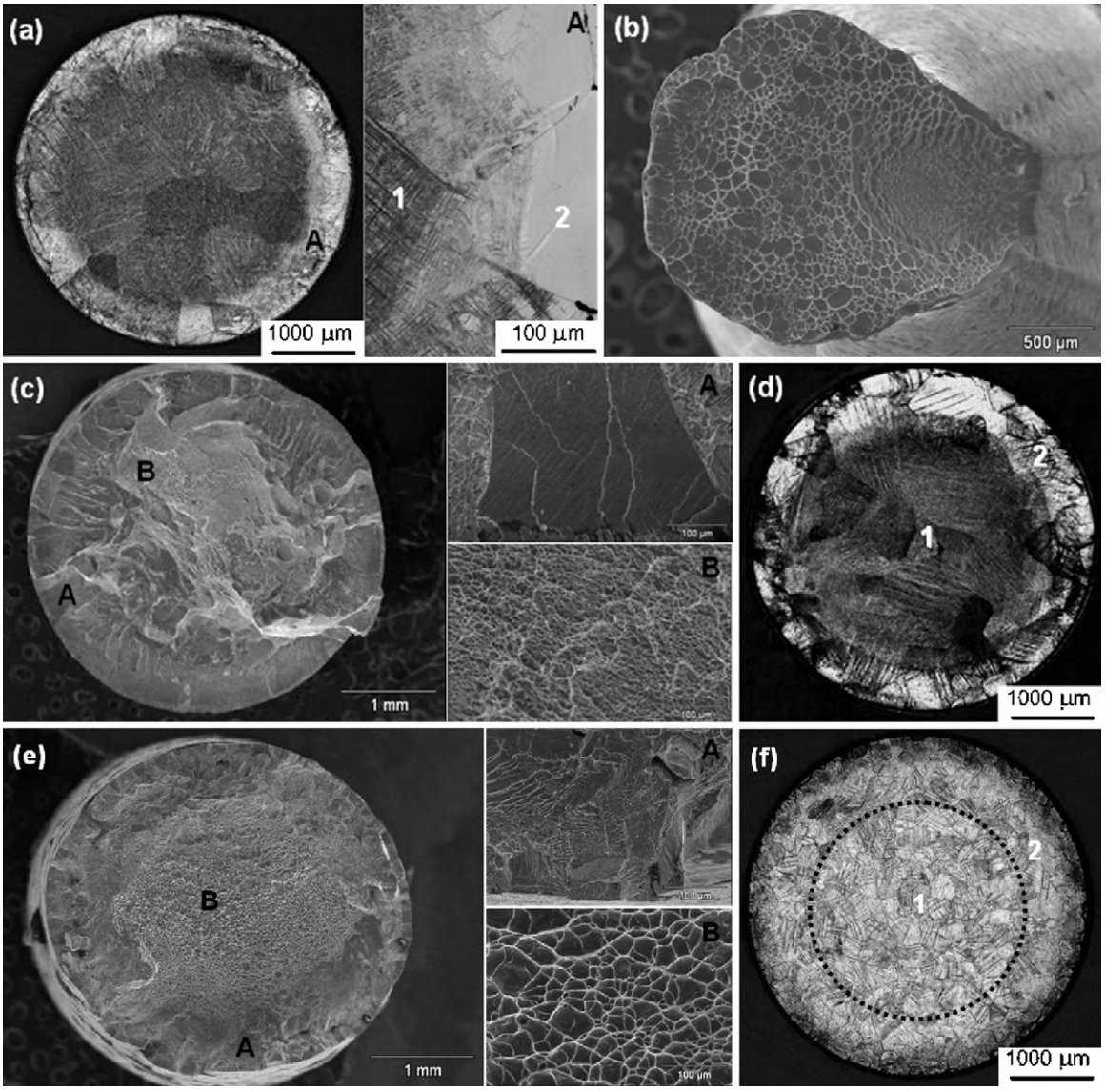

Fig. 10. Tensile test specimens of water-quenched alloys. (a) Microstructure just below the fracture surface of the Ti–25Nb alloy. The detail at the right of this figure shows a small amount of the β phase, which was retained throughout the periphery of the cross-section. The hardness average value in this region was 366 HV (2), whereas in the region formed by α″ was 187 HV (1). (b) Fracture surface of theTi–25Nb–2.5Ta alloy. (c) Fracture surface of the Ti–25Nb–5Ta alloy and (d) the corresponding microstructure just below it. The details A and B at right of (c) present regions of the fracture surface under higher magnification. (d) Shows α″ phase formed inside of the cross-section and retained β throughout its periphery. The hardness average values of each region were 180 HV (1) and 302 HV (2), respectively. (e) Fracture surface of the Ti–35Nb–5Ta alloy and (f) the corresponding microstructure just below it. The details A and B at right of (e) present regions of the fracture surface under higher magnification. The dot circle in (f) separates the cross-section of the specimen inside two regions with different hardness average values: 150 HV (1) and 260 HV (2).

collapse of $\{1\,1\,1\}_\beta$ atomic planes in the β phase [47]. Taking WQ specimens of composition Ti–35Nb–5Ta and Ti–35Nb–7.5Ta as an example, oxygen contents of their peripheral zones were 0.193 wt.% and 0.115 wt.%, respectively; the specimen containing 5%Ta presented 28% of reduction in area, whereas the value of the specimen containing 7.5%Ta was 65%, Fig. 9. This suggests that a link may exist between the higher oxygen content and the low reduction in area in the Ti–35Nb–5Ta specimen. In fact, its microstructure just below the fracture surface presented two regions with different hardness average values: 260 (peripheral zone) and 150 (central region); Fig. 10f shows the two regions separated by the dot circle. Consequently, this higher value in hardness may be attributed to oxygen interstitial solid solution strengthening of the β phase. However, it is not clear if the oxygen contamination is the only factor for the drop in the reduction in area, causing deterioration of the mechanical behavior. At least, the oxygen content do not seem to be enough to completely suppress the ω formation, since TEM analysis revealed the presence of its precipitates in this specimen, Fig. 7a and b.

Considering again the WQ samples containing 25% Nb, when the Ta content was 2.5%, the microstructure was basically formed by α″ (Fig. 11a) and the fracture surface observed was completely dimpled (Fig. 10b). The specimen containing 7.5% Ta presented the same fracture mode; its XRD peaks show a direct indication of β retention (Fig. 11c). Both specimens presented a relatively uniform distribution of the β and α″ phases along the microstructures. The specimen of composition Ti–25Nb–5Ta, on the other hand, presented two different fracture modes (Fig. 10c). The central region (labeled B) presented a transgranular dimpled fracture surface, whereas throughout the periphery of the cross-section (labeled A), many facets are seen. Hardness measurements were performed just below the fracture surface, and the average value obtained in the peripheral zone was 302 HV. The central region of the specimen, composed of α″, showed considerably lower hardness (180 HV).

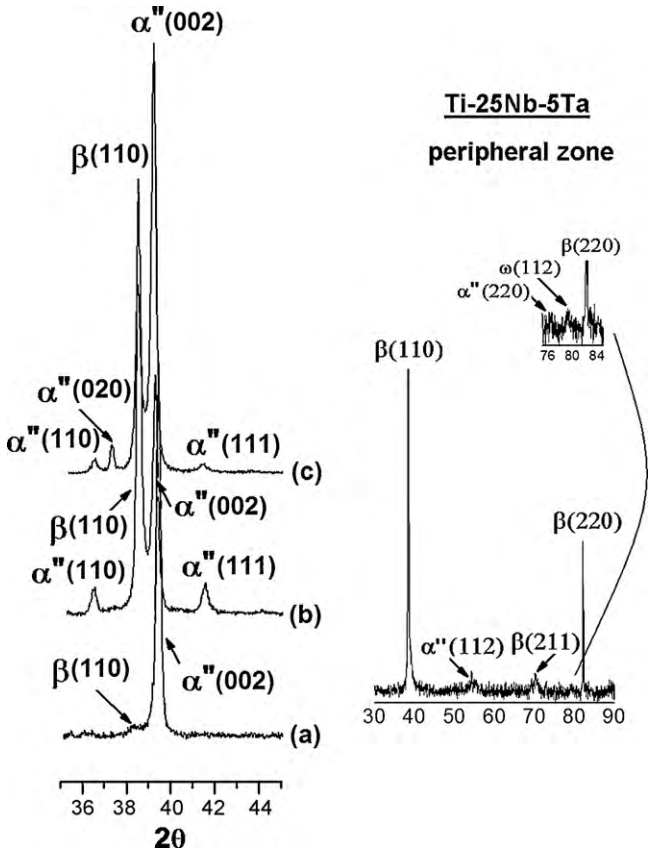

Fig. 11. X-ray diffraction patterns of the cross-sections below the fracture surfaces of (a) Ti–25Nb–2.5Ta, (b) Ti–25Nb–5Ta and (c) Ti–25Nb–7.5Ta. The detail on the right-hand side corresponds to the X-ray diffraction pattern of the peripheral zone of the Ti–25Nb–5Ta alloy, where ω phase was identified. Lattice parameters (nm) of the identified phases: α″ (a = 0.2856, b = 0.4830 and c = 0.4573); β (a = 0.3310); and ω (a = 0.4646 and c = 0.2820).

The facets observed show that intergranular fracture has occurred; according to Hon et al. [30], this may occur in Ti–Nb alloys due to the presence of the ω phase. At first the X-ray diffraction analysis identified α″ and β (Fig. 11b), but the different values of hardness between peripheral and central areas of the cross-section encouraged specific X-ray analysis of the peripheral zone that detected the presence of the ω phase (see detail in Fig. 11). A similar fracture surface was also observed in the WQ specimen of composition Ti–35Nb–5Ta, Fig. 10e. The WQ specimen of composition Ti–25Nb–5Ta presented poor ductility, higher yield strength and lower tensile strength when compared to the other alloys (Fig. 9b). The ω precipitation in the periphery may strengthen the material and retard yielding. Afterwards, the presence of ω may preclude plastic deformation and favor cracking that leads to macroscopic brittleness and premature failure. Taken together, these findings suggest that the non-systematic change in the mechanical properties is a consequence of a combination of the oxygen contamination and irregular ω phase distribution in the periphery of the specimens.

4. Conclusions

The following conclusions can be drawn from the present study:

(a) All samples in the FC condition presented the α and β phases; the volume fraction of α was considerably high for those containing 25 and 30%Nb. In the AC condition, samples containing 25%Nb presented the α and α″ phases; β retention was not observed in Ti–25Nb and Ti–25Nb–2.5Ta samples. The other compositions exhibited fine α precipitation in the β matrix, except Ti–35Nb–7.5Ta. High density of ω precipitates was observed in FC and AC samples. The hardness and elastic modulus profiles of FC and AC samples are described by an initial rise and subsequent fall, as the content of alloying elements increases. The highest hardness values are achieved with low concentrations of alloying elements in the AC condition, since the cooling rate of 11 °C/s hinders nucleation and growth of α and favors formation of the harder metastable phases. In both FC and AC conditions, ω precipitation had a major influence on the elastic modulus and hardness values of the samples.

(b) The microstructures of OQ and WQ alloys containing 25 and 30 wt.%Nb are basically formed by α″ martensite. Ti–35Nb–7.5Ta is the only composition in which the β phase was entirely retained. Reduced ω precipitation and α suppression were responsible for low values of elastic modulus in OQ and WQ alloys, and a continuous decrease was observed due to higher β retention as the content of alloying elements increases. The lowest elastic modulus was obtained with the alloy of composition Ti–35Nb–7.5Ta in the WQ condition. Regarding hardness, a dropping trend was noticed when Ta is added to Ti–Nb alloys; the alloy Ti–35Nb–7.5Ta presented solid solution strengthening.

(c) Mechanical properties of quenched alloys can be summarized by high ductility and relatively low strength. Strength decreased with increasing Nb and Ta contents but the reduction in area seems to be independent of the additions. Some alloys presented low reduction in area probably as a consequence of the irregular ω phase distribution and the oxygen contamination. These alloys presented β phase retention preferably at the periphery of specimens, which is attributed to the fall of M_S due to the influence of the cooling rate in Ti-alloys containing Nb and Ta elements, since the higher cooling rate is obtained superficially, and the effect of the oxygen contamination.

Acknowledgements

The authors would like to acknowledge the financial support of the Foundation for the Support of Research of the State of São Paulo (FAPESP) and the Brazilian Synchrotron Light Laboratory (LNLS) for the use of their microscopy laboratories.

References

[1] R. Mythili, V. Thomas Paul, S. Saroja, M. Vijayalakshmi, V.S. Raghunathan, Mater. Sci. Eng., A 390 (2005) 299–312.
[2] C.J. Boehlert, Mater. Sci. Eng., A 267 (1999) 82–98.
[3] K. Wang, Mater. Sci. Eng., A 213 (1996) 134–137.
[4] M. Niinomi, Sci. Tech. Adv. Mater. 4 (2003) 445–454.
[5] Y. Song, R. Yang, Z.-X. Guo, Mater. Trans. 43 (2002) 3028–3031.
[6] E. Takahashi, T. Sakurai, S. Watanabe, N. Masahashi, S. Hanada, Mater. Trans. 43 (2002) 2978–2983.
[7] M. Niinomi, Metall. Mater. Trans. A 33 (2002) 477–486.
[8] D. Kuroda, M. Niinomi, M. Morinaga, Y. Kato, T. Yashiro, Mater. Sci. Eng., A 243 (1998) 244–249.
[9] G. Yang, T. Zhang, J. Alloys Compd. 392 (2005) 291–294.
[10] M. Niinomi, Mater. Sci. Eng., A 243 (1998) 231–236.
[11] M. Long, H.J. Rack, Biomaterials 19 (1998) 1621–1639.
[12] Y. Okasaki, Y. Ito, K. Kyo, T. Tateishi, Mater. Sci. Eng., A 213 (1996) 138–147.
[13] H.E. Cook, Acta Metall. 22 (1974) 239–247.
[14] A. Lenain, N. Clément, M. Véron, P.J. Jacques, J. Mater. Eng. Perform. 14 (2005) 722–727.
[15] X. Tang, T. Ahmed, H.J. Rack, J. Mater. Sci. 35 (2000) 1805–1811.
[16] A.V. Dobromyslov, G.V. Dolgikh, J. Dutkiewicz, T.L. Trenogina, Arch. Metall. Mater. 51 (2006) 547–550.
[17] A.V. Dobromyslov, Adv. Mater. Sci. 8 (2008) 37–42.
[18] E.W. Collings, Titanium alloys, in: Materials Properties Handbook, ASM Materials Park, 1994.
[19] A.V. Dobromyslov, V.A. Elkin, Scr. Mater. 44 (2001) 905–910.
[20] A.V. Dobromyslov, V.A. Elkin, Mater. Sci. Eng., A 438–440 (2006) 324–326.
[21] Y.L. Zhou, M. Niinomi, T. Akahori, Mater. Sci. Eng., A 371 (2004) 283–290.

[22] S.G. Fedotov, T.V. Chelidze, Yu.K. Kovneristyy, V.V. Sanadze, Fiz. Met. Metalloved. 62 (1986) 328–332.
[23] K.A. Bywater, J.W. Christia, Philos. Mag. 25 (1972) 1249–1273.
[24] P.L. Ferrandini, F.F. Cardoso, S.A. Souza, C.R. Afonso, R. Caram, J. Alloys Compd. 433 (2007) 207–210.
[25] P.J. Bania, JOM 46 (1994) 16–19.
[26] G. Lütjering, J.C. Williams, Titanium, first ed., Springer-Verlag, Berlin, 2003.
[27] M. Abdel-Hady, H. Fuwa, K. Hinoshita, H. Kimura, Y. Shinzato, M. Morinaga, Scr. Mater. 57 (2007) 1000–1003.
[28] P.R. Rios, F. Siciliano Jr., H.R.Z. Sandim, R.L. Plaut, A.F. Padilha, Mater. Res. 8 (2005) 225–238.
[29] E. Breslauer, A. Rosen, Mater. Sci. Technol. 7 (1991) 441–446.
[30] Y.-H. Hon, J.-Y. Wang, Y.-N. Pan, Mater. Trans. 44 (2003) 2384–2390.
[31] W.F. Ho, C.P. Ju, J.H. Chern Lin, Biomaterials 20 (1999) 2115–2122.
[32] Y.L. Zhou, M. Niinomi, T. Akahori, Mater. Sci. Eng., A 384 (2004) 92–101.
[33] C.M. Lee, C.P. Ju, J.H. Chern Lin, J. Oral Rehab. 29 (2002) 314–322.
[34] K.S. Jepson, A.R.G. Brown, J.A. Gray, Transformation in titanium–niobium and titanium–aluminium alloys, in: R.I. Jaffee (Ed.), Science, Technology and Application of Titanium, Pergamon Press, Oxford, 1970, pp. 677–690.
[35] D.L. Moffat, D.C. Larbalestier, Met. Trans. A 19 (1988) 1677–1686.
[36] T.W. Duerig, G.T. Terlinde, J.C. Williams, Met. Trans. A 11 (1980) 1987–1998.
[37] D.L. Moffat, D.C. Larbalestier, Met. Trans. A 19 (1988) 1687–1694.
[38] Y. Mantani, M. Tajima, Mater. Sci. Eng., A 438 (2006) 315–319.
[39] Z. Fan, Scr. Metall. Mater. 29 (1993) 1427–1432.
[40] Y.L. Hao, M. Niinomi, D. Kuroda, K. Fukunaka, Y.L. Zhou, R. Yang, A. Suzuki, Metall. Mater. Trans. A 34 (2003) 1007–1012.
[41] E.W. Collings, The Physical Metallurgy of Titanium Alloys, ASM, Metals Park, 1984.
[42] L.A. Matlakhova, A.N. Matlakhova, S.N. Monteiro, S.G. Fedotov, B.A. Goncharenko, Mater. Sci. Eng. A 393 (2005) 320–326.
[43] G.E. Dieter, Mechanical Metallurgy, 3rd ed., McGraw-Hill, New York, 1986.
[44] F.H. Froes, C.F. Yolton, J.M. Capenos, M.G.H. Wells, J.C. Williams, Met. Trans. A 11 (1980) 21–31.
[45] H.Y. Kim, S. Hashimoto, J.I. Kim, T. Inamura, H. Hosoda, S. Miyazaki, Mater. Sci. Eng., A 417 (2006) 120–128.
[46] J.I. Kim, H.Y. Kim, H. Hosoda, S. Miyazaki, Mater. Trans. 46 (2005) 852–857.
[47] M. Abdel-Hady, K. Hinoshita, M. Morinaga, Scr. Mater. 55 (2006) 477–480.